Letter

Predicting the Ion Desolvation Pathway of Lithium Electrolytes and Their Dependence on Chemistry and Temperature

John Holoubek, Artem Baskin,* John W. Lawson, Hridayanand Khemchandani, Tod A. Pascal, Ping Liu,* and Zheng Chen*

Cite This: *J. Phys. Chem. Lett.* 2022, 13, 4426−4433

Read Online

ACCESS | 📊 Metrics & More | 📑 Article Recommendations | 🆂�🅸 Supporting Information

ABSTRACT: To better understand the influence of electrolyte chemistry on the ion-desolvation portion of charge-transfer beyond the commonly applied techniques, we apply free-energy sampling to simulations involving diethyl ether (DEE) and 1,3-dioxoloane/1,2-dimethoxyethane (DOL/DME) electrolytes, which display bulk solvation structures dominated by ion-pairing and solvent coordination, respectively. This analysis was conducted at a pristine electrode with and without applied bias at 298 and 213 K to provide insights into the low-temperature charge-transfer behavior, where it has been proposed that desolvation dominates performance. We find that, to reach the inner Helmholtz layer, ion-paired structures are advantageous and that the Li$^+$ ion must reach a total coordination number of 3, which requires the shedding of 1 species in the DEE electrolyte or 2−3 species in DOL/DME. This work represents an effort to predict the distinct thermodynamic states as well as the most probable kinetic pathways of ion desolvation relevant for the charge transfer at electrochemical interfaces.
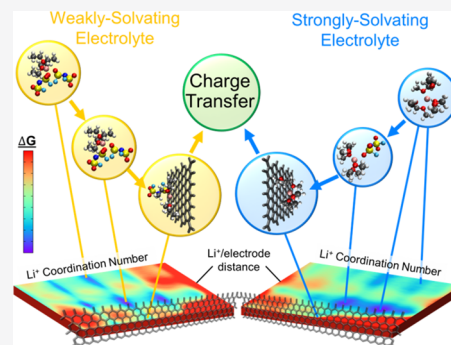
Secondary batteries based on Li chemistries have become an indispensable technology for modern portable electronics. However, to enable the efficient utilization of renewable energy technologies for electric vehicles and advanced air mobility, considerable effort has been put into improving the energy density, power density, and operating versatility of these devices.[1−4] Of note, the electrochemical kinetics of commercial batteries are currently insufficient to provide charging times comparable to standard refueling periods and to deliver power at reduced operating temperatures.[2−11] Additionally, these operating issues are expected to be exacerbated with the introduction of Li metal anodes, which promise improved cell energy density, but introduce internal shorting and poor cyclability concerns at high current rates or reduced temperature.[12−14] To alleviate these concerns, substantial effort must be placed into understanding and addressing the electrochemical rate-limiting steps of current and next-generation secondary batteries.

Generally, the limiting kinetic factors of Li-based secondary batteries employing aprotic electrolytes are considered to be (1) diffusion of Li$^+$ within the bulk of the electrode materials, (2) migration of Li$^+$ through the solid-electrolyte-interphase (SEI), (3) diffusion of Li$^+$ through the electrolyte bulk, and (4) charge-transfer at the electrode interphase, which has been suggested to be dominated by Li$^+$ desolvation.[8,15,16] The latter three of these processes are highly sensitive to electrolyte chemistry, where there is a well-established effort to maximize the Li$^+$ transference number and ionic conductivity in solution while forming low-impedance SEI products on each

electrode.[5,6,9,17] However, recently, a growing amount of evidence has suggested that the charge-transfer process is also highly influential in the kinetic performance of Li-based batteries, which is largely defined by the Li$^+$ solvation structure in the electrolyte.[14,18−20] It is also important to note that this charge-transfer relationship is well-accepted in batteries employing multivalent charge carriers.[21−25] While there are many methods by which bulk ion transport and SEI chemistry can be characterized, the Li$^+$ desolvation process and the system factors which dictate its energetics are still largely unknown and therefore are under-studied.

While the interplay between impedance contributors arising from ion desolvation, SEI, and bulk electrolyte transport is still largely unclear under standard operating temperatures, it has been suggested that the desolvation impedance is dominant at ultralow operating temperatures (<−20 °C).[8,26] This heightened charge-transfer barrier at ultralow temperatures has been demonstrated to lead to insufficient power delivery and, in the case of Li metal anodes, to lead to extremely reduced cycling efficiency and internal cell shorting as a result of dendritic growth.[14,27,28] Our recent work has concluded that the
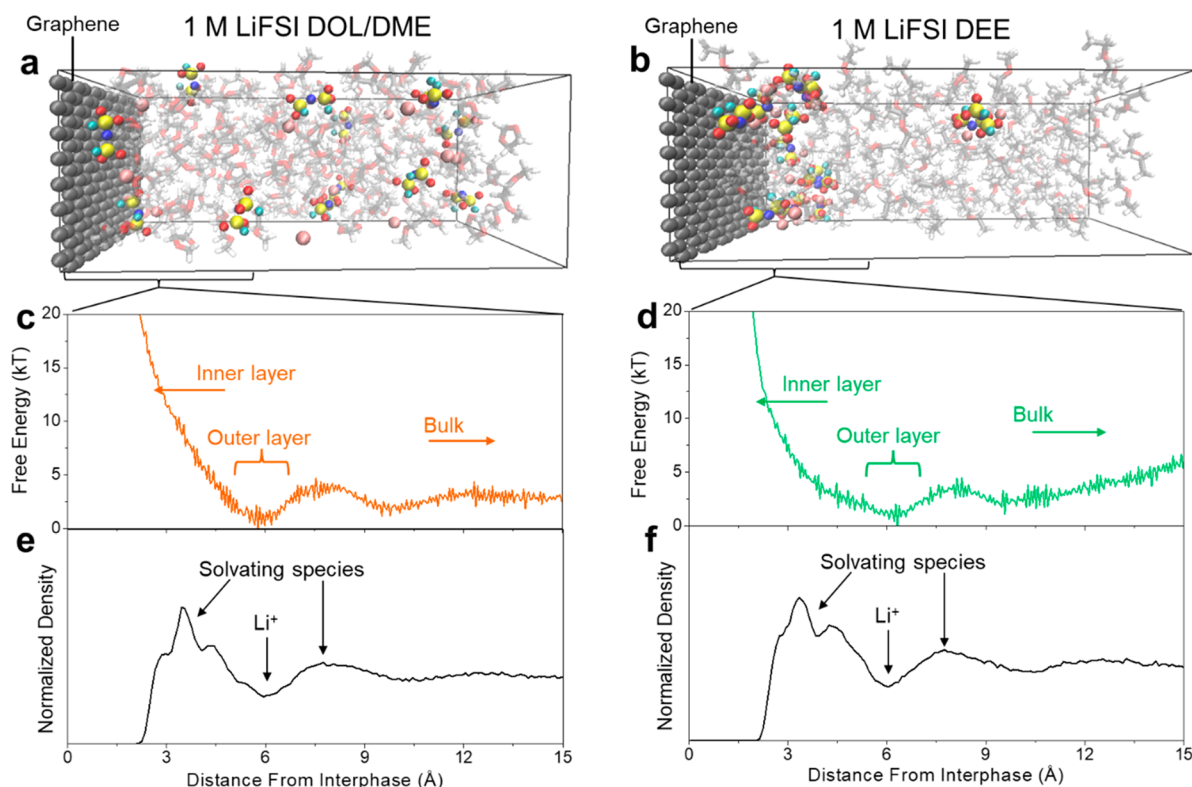
Figure 1. Snapshot of the equilibrated electrolyte/graphene simulation cells at 298 K employing (a) 1 M LiFSI DOL/DME and (b) 1 M LiFSI DEE. 1D free energy profile of Li$^+$ as a function of distance from the graphene electrode fixed at the plane $z = 0$ in (c) 1 M LiFSI DOL/DME and (d) 1 M LiFSI DEE. Normalized system number density as a function of distance from the graphene electrode taken from equilibration trajectories in (e) 1 M LiFSI DOL/DME and (f) 1 M LiFSI DEE.

introduction of ion-pairing and weakly coordinating solvent within the electrolyte may significantly reduce this desolvation impedance at reduced temperatures, enabling the reversible cycling of Li down to −60 °C.[14] Despite these trends, many mechanistic questions still remain, particularly in the case of Li-based systems.

Though there is a clear correlation in the literature between the electrolyte's bulk solvation structure and its temperature-dependent charge-transfer, the precise details of the desolvation process at the electrode are relatively unclear. From a Marcus theory perspective, both thermodynamic and kinetic factors may give rise to this temperature dependence.[29−31] From a thermodynamic standpoint, Wang et al. recently proposed that the Li$^+$ solvation structure at the interphase directly defines the electrochemical exchange entropy between solvated Li$^+$ and metallic Li/lithiated host.[32] Of note, ion-pairing was demonstrated to reduce the temperature dependence of Li/Li$^+$ exchange. From a kinetic standpoint, the stiffness of the Li$^+$ solvation shell at the interphase directly dictates the reorganization process required for charge-transfer. In this regard, multiple works have concluded that ion-pairing in solution generally appears to reduce overall impedance due to a reduced barrier for nuclear motion of the solvation shell at the interphase.[19,22,31] Though Li$^+$/solvent binding energy calculated via density functional theory is often used as a proxy for interphasial desolvation energy,[14,18,33] this analysis neglects the effects of a biased electrode, solvation shell speciation, and many-body effects on the desolvation route, which suggests that a more sophisticated methodology is necessary.

In this work, we aim to gain a more precise understanding of the interphasial speciation and desolvation mechanics of the solvated Li$^+$ ion via accelerated molecular dynamics (MD) simulations employing a previously established metadynamics-based approach.[22] Our approach is motivated by the fact that the complexity of the desolvation process requires an understanding of the entire electrode/electrolyte phase space, including states beyond what is thermally accessible through standard MD simulations. By exploring the multidimensional phase space along specific reaction coordinates this free energy sampling technique allows us to uncover the essential features and details of the ion desolvation process and their quantitative characteristics.[22,34,35] Though we acknowledge that the employment of polarizable or reactive force fields may provide a higher level of sophistication to such analysis the classical force field employed here is necessary to operate within the time scales necessary for such sampling (Table S2).

Specifically, we conduct simulations of 1 M lithium bis(fluorosulfonyl)imide (LiFSI) in 1,3-dioxolane/1,2-dime-thoxyethane (DOL/DME) and 1 M LiFSI in diethyl ether (DEE) in contact with a model solid electrode, using a combination of reaction coordinates that includes the distance between Li$^+$ and the electrode as well as the speciation of the solvation shell as a tool to probe desolvation dynamics at the interphase. These two model electrolytes were applied in our previous experimental work, where the heavily ion-paired DEE electrolyte displayed a substantially reduced desolvation impedance and correspondingly favorable low-temperature performance compared to the DOL/DME system, which displayed solvent-dominated Li$^+$ coordination.[14] Considering the aforementioned thermodynamic and kinetic factors
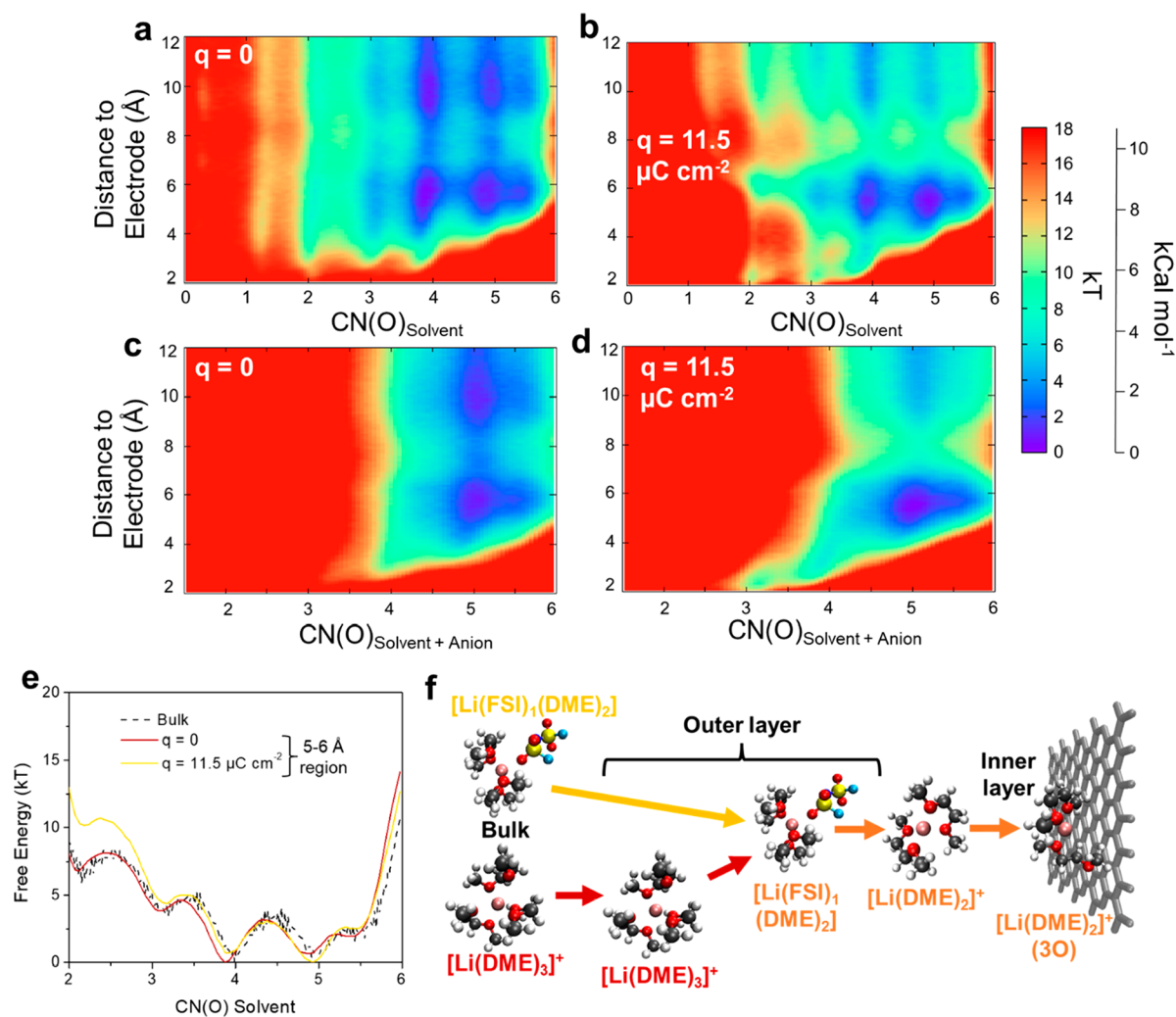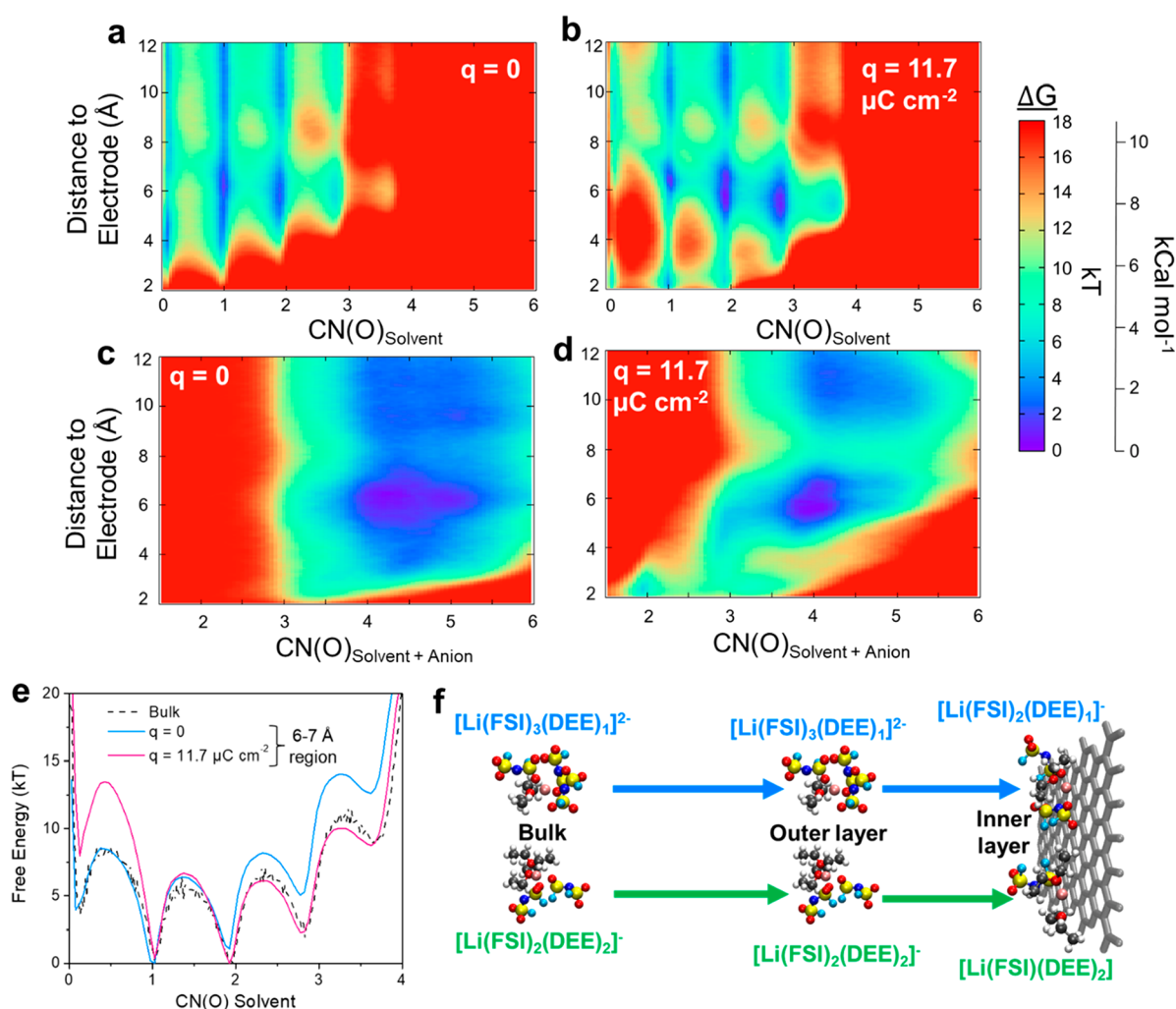
Figure 2. 2D free energy profiles of 1 M LiFSI DOL/DME/graphene cells at 298 K as a function of Li$^+$/graphene distance and coordination number. Profiles with respect to Li$^+$/solvent oxygen coordination number with a graphene charge of (a) 0 and (b) 11.5 μC cm^{-2}. Profiles with respect to Li$^+$/solvent and anion oxygen coordination number with a graphene charge of (c) 0 and (d) 11.5 μC cm^{-2}. (e) 1D free energy profiles as a function of Li$^+$/solvent oxygen CN in the bulk electrolyte (Supporting Information) and within the outer layer region (integrated over 5−6 Å) of the 2D profiles. (f) Visualized Li$^+$ desolvation process of in 1 M LiFSI DOL/DME at 298 K.

dictating charge-transfer, this highly disparate electrochemical performance may originate from an explicit change in preferred solvation structure at the interphase at reduced temperature, or the inherent temperature dependence of the kinetic desolvation barrier(s) along the previously established reaction coordinates. Hence, we aim to better understand the origin and energetic implications of electrolyte chemistry, interphasial bias, and reduced system temperature on the solvation states present in the bulk, the electrode double-layer, and their corresponding transformations as the charge carrier proceeds to the interphase.

Before assessing the interphasial solvation structures and solvation dynamics at the interphase, the coordinating environments of 1 M LiFSI DOL/DME and 1 M LiFSI DEE were first analyzed in the bulk (Supporting Information). As shown in Figure S1, parts a and c, we found that the primary Li$^+$ solvation shell in the bulk DOL/DME system is dominated by coordinating DME oxygen atoms, which predicts an average solvation structure of $[\text{Li-}(\text{DME})_{2.2}(\text{DOL})_{0.35}(\text{FSI})_{0.46}]^{0.54}$ after equilibration. Notably, DME contains two oxygens per molecule and must be

multiplied by 2 to retrieve the correct Li$^+$/O coordination number (CN). Conversely, the DEE electrolyte results in a heavily ion-paired solvation structure of $[\text{Li-}(\text{DEE})_{1.8}(\text{FSI})_{2.3}]^{-1.3}$ on average. The 1D free energy profiles for the Li$^+$ coordination environment of each system indicate that minima exist for $[\text{Li}(\text{DME})_{2.5}]^+$ (5 DME oxygens) and $[\text{Li}(\text{DME})_2(\text{FSI})]$ (four DME, one FSI oxygen) states in 1 M LiFSI DOL/DME, whereas the DEE system primarily supports $[\text{Li}(\text{DEE})_1(\text{FSI})_3]^{2-}$ and $[\text{Li}(\text{DEE})_2(\text{FSI})_2]^-$ states. It is also worth noting that the DOL/DME system was found to favor a total coordination number of ∼5, as opposed ∼4 in DEE, reflective of the increased sterics in DEE.

After bulk analysis, the electrolyte systems were then placed in contact with a pristine graphene electrode similar to previous work.[22] No passivating layer was included on the surface of the electrode due to the unclear speciation, spatial orientation, and structure of such a layer at the angstrom scale, which we believe would overcomplicate the interphasial solvation analysis. While the structure and chemistry of said passivating interphase have been shown to play a significant role in the energetics of interphasial ion processes, we propose

Figure 3. 2D Free energy profiles of 1 M LiFSI DEE/graphene cells at 298 K as a function of Li$^+$/graphene distance and coordination number. Profiles with respect to Li$^+$/solvent oxygen coordination number with a graphene charge of (a) 0 and (b) 11.5 μC cm^{-2}. Profiles with respect to Li$^+$/solvent and anion oxygen coordination number with a graphene charge of (c) 0 and (d) 11.5 μC cm^{-2}. (e) 1D free energy profiles as a function of Li$^+$/solvent oxygen CN in the bulk electrolyte (Supporting Information) and within the outer layer region (integrated over 6−7 Å) of the 2D profiles. (f) Visualized Li$^+$ desolvation process of in 1 M LiFSI DEE at 298 K.

that the designed system is appropriate to investigate the role of electrolyte chemistry and temperature on desolvation.[36,37] Future investigation of such passivating layers on desolvation behavior requires a more thorough understanding of the interphasial environment and may lead to additional insights.

Snapshots of the equilibrated cells for 1 M LiFSI DOL/DME and 1 M LiFSI DEE are shown in parts a and b of Figure 1, with more details provided in the Supporting Information. For the remainder of this work, we will differentiate between various regions within these interphasial MD simulations that describe specific energetic states of interest for the Li$^+$ ion and its solvation. These regions are labeled in parts c and d of Figure 1 as the bulk electrolyte (> ∼ 10 Å from the graphene sheet), the outer Helmholtz double layer (∼5−7 Å), and the inner Helmholtz layer (<3 Å). It can be seen in the 1D free energy profiles that the free energy minima of Li$^+$ in both electrolytes in contact with neutral ($q = 0$) graphene are in the outer Helmholtz layer. We find that the low density region corresponds to preferred Li$^+$ location, whereas the densified regions consist of its solvent and FSI$^-$ (Figure S2). We believe the degree to which these solvating species must be displaced for Li$^+$/electrode adsorption (i.e., entering the inner Helmholtz

layer) preceding charge-transfer is of high interest to the electrochemical performance of each system.[16,18,26]

To understand the dynamics of the Li$^+$ solvation shell at the interphase, free energy analysis was conducted on cells with neutral and negatively charged graphene electrodes at 298 K. 11.5 μC cm^{-2} was chosen as the graphene charge (see details in the Supporting Information), which is a similar magnitude to previous MD works involving charged electrodes.[38] The 2-D energetic surfaces were resolved with respect to Li$^+$ distance to graphene as well its coordination environment, inferring speciation from differences between preferred total coordination number and solvent specific coordination number. The inner layer was found to be energetically inaccessible for Li$^+$ (Li$^+$ < ∼ 2.5 Å from the electrode) unless a negative charge was applied to the electrode (Figure 2a-d). By comparing the 1D solvation profile of the bulk and integrated outer layer (Figure 2e), we find that both the $[Li(DME)_{2.5}]^+$ (i.e., a complex with $CN(O)_{DME} = 5$, where two DME molecules provide four oxygens, and another DME molecule provides 1 oxygen) and $[Li(DME)_2(FSI)]$ ($CN(O)_{DME} = 4$) states are accessible in either region, regardless of the interphase charge. However, we find that the $[Li(DME)_{2.5}]^+$ structure does not
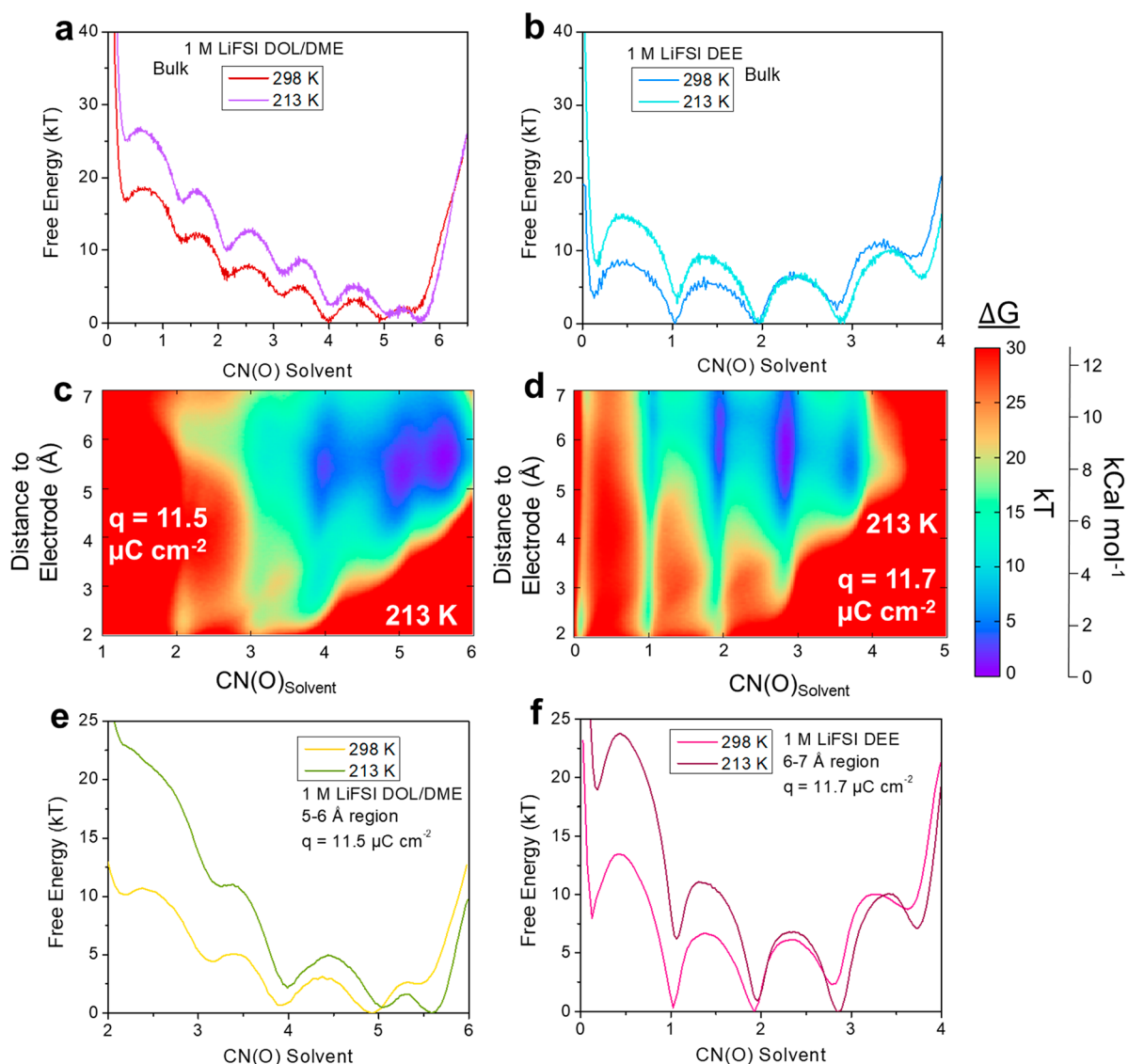
Figure 4. 1D free energy profiles with respect to Li$^+$/solvent oxygen coordination number at 298 and 213 K in (a) 1 M LiFSI DOL/DME and (b) 1 M LiFSI DEE. 2D Free energy profiles of electrolyte/charged graphene cells at 213 K as a function of Li$^+$/graphene distance and solvent oxygen coordination number in (c) 1 M LiFSI DOL/DME and (d) 1 M LiFSI DEE. 1D free energy profiles as a function of Li$^+$/solvent oxygen CN within the outer layer region (integrated over labeled region) of the 2D profiles at 298 and 213 K in (e) 1 M LiFSI DOL/DME and (f) 1 M LiFSI DEE.

approach the electrode from the outer layer. Instead, the low energy pathway requires generation of the ion-paired [Li-(DME)$_2$(FSI)] state (Figure 2b,d), which is consistent with previous conclusions made when considering the Mg(TFSI)$_2$/THF system.[22] Furthermore, comparing the 2-D free energy spectra with respect to solvent coordination number only (Figure 2b) and both solvent and anions (Figure 2d), we find that in order for the Li$^+$ to reach the inner layer in DME, the [Li(DME)$_2$(FSI)] (CN(O)$_{DME}$ = 4) complex must undergo two desolvation events. Specifically, the [Li(DME)$_2$(FSI)] complex must first shed its coordinating FSI$^-$ to exit the outer layer and arrive within ~5 Å of the electrode, after which the [Li(DME)$_2$]$^+$ (CN(O)$_{DME}$ = 4) complex must then shed one final DME oxygen to fully reach the inner layer. Figure 2f illustrates this low energy pathway in detail.

The interphasial solvation dynamics of 1 M LiFSI DEE diverge significantly from those of DOL/DME, as demonstrated by the presence of highly ion-paired bulk structures in the outer layer. It is also readily apparent that the number of

the coordinating FSI$^-$ is of significance to the distance Li$^+$ can approach the graphene interphase, where [Li(DEE)$_1$(FSI)$_3$]$^{2-}$ and [Li(FSI)$_4$]$^{3-}$ are able to approach the electrode at much closer distances than complexes with higher DEE compositions. However, as the fully anion coordinated complex [Li(FSI)$_4$]$^{3-}$ is inaccessible in the bulk, we believe this is highly unlikely to exist experimentally. Moreover, the consistency between the supported solvation states in the bulk and the outer layer is maintained when a negative charge of 11.7 μC cm^{-2} is applied to the graphene electrode (Figure 3b,e). It was also found that the adsorbed states are stabilized by the application of negatively charged graphene, where [Li(DEE)$_1$(FSI)$_3$]$^{2-}$ and [Li(DEE)$_2$(FSI)$_2$]$^-$ outer layer states proceeded to the inner layer without the removal of any coordinating DEE (Figure 3b,d). When cross-referenced to the free energy surfaces with respect to total coordination number, it was found that this Li$^+$/graphene adsorption is made possible by the removal of one FSI$^-$ from the [Li-(DEE)$_1$(FSI)$_3$]$^{2-}$ or [Li(DEE)$_2$(FSI)$_2$]$^-$ complexes. Consider-

ing these observations, the predicted desolvation process in the DEE electrolyte at 298 K is illustrated in Figure 3f.

After establishing the predicted desolvation processes in the electrolytes of interest at 298 K, we conducted a similar analysis 213 K in order to understand the impact of reduced temperature on this process. First, the impact of this temperature reduction on the Li^+ solvation structure in the bulk electrolyte was assessed, as the configuration of this structure has been experimentally correlated to changes in charge-transfer kinetics.[14,18,19,21,26,31] As shown in Figure 4a, the DOL/DME electrolyte was found to adopt a substantially different Li^+ coordination environment than at 298 K, and it is dominated by solvent interactions, where Li^+/FSI^- ion-pairing in solution ($CN(O)_{DME} = 4$) is no longer thermodynamically accessible. Instead, a new favorable solvent coordination state appears, corresponding to an oxygen coordination number of ~5.7, implying that the previously dangling oxygen of the third coordinating DME begins to participate in solvation. The noninteger coordination number value is likely an artifact of the definition of the coordination number as a continuous variable (Supporting Information), so that we consider the ~5.7 CN state to be effectively 6 CN. The 1D free energy spectra with respect to total coordination number of the DOL/DME system also supports this finding, where the minima is again shifted from ~5 at 298 K to 6 at 213 K (Figure S3b). The 1 M LiFSI DEE electrolyte was found to undergo a similar transformation, where the previously prevalent $[Li(DEE)_1(FSI)_3]^{2-}$ and $[Li(DEE)_2(FSI)_2]^-$ states at 298 K shift to $[Li(DEE)_2(FSI)_2]^-$ and $[Li(DEE)_3(FSI)_1]$ states at 213 K. However, unlike the DOL/DME system, the total coordination number of the DEE electrolyte was found to be unchanged by the reduced temperature (Figure S3b). The effect of temperature on bulk coordination may be related to the thermally accessible vibrational states of each coordinating molecule in solution. In the DOL/DME system, the reduced temperature may favor more the electrostatically driven coordination of the third DME's second oxygen (enthalpically preferred) which otherwise dangles due to the increased entropic preference at 298 K. Additionally, the tendency of both systems to skew toward solvent coordination at reduced temperature may reveal an intrinsic difference in the ratio of entropic loss to enthalpic gain between the coordination of solvents and FSI^-.

To assess whether this shift in coordination environment has a meaningful effect on the interphasial solvation dynamics at 213 K, we conducted a similar 2-D free energy analysis to the outer layer and inner layer regions of identical graphene cells (Supporting Information). Similar to the 298 K simulations, we find that the inner layer Li^+ states are only accessible when negative charge is applied to the electrode (Figure S4). As shown in Figure 4c, it is once again observed that at least one Li^+/FSI^- pair is required to approach the interphase in the DOL/DME system. However, unlike at 298 K, the simulations do not indicate that the $[Li(DME)_2(FSI)]$ is supported in the outer layer. Instead, the same $[Li(DME)_3]^+$ ($CN(O)_{DME} = 6$) state was found to persists from the bulk (Figure 4e). This mismatch between the preferred outer layer solvation states and the path necessary for Li^+ to reach the inner layer indicates that a solvation transition must occur between the fully solvent coordinated $[Li(DME)_3]^+$ ($CN(O)_{DME} = 6$) and $[Li(DME)_2(FSI)_1]$ ($CN(O)_{DME} = 4$) states, which involves the full replacement of a coordinating DME molecule with an FSI^-. Though the driving force provided by the electrode

during charge-transfer to such a transition is relatively unclear, this process is predicted to involve overcoming an activation energy of >5 kT (Figure 4e). Alternatively, charge-transfer directly from the $[Li(DME)_3]^+$ system is possible, but would likely require substantially increased driving force given the distance between Li^+ and the electrode, which is highly influential in outer-sphere kinetics.[29,30] We hypothesize that this arduous desolvation pathway may be the source of the substantial electrochemical performance degradation of the DOL/DME system at reduced temperatures.[14,27,28]

On the other hand, the DEE system was found to maintain a relatively simple desolvation process, where the $[Li(DEE)_2(FSI)_2]^-$ complex is supported in the outer layer (Figure 4f), only requiring the ejection of 1 FSI^- molecule for Li^+/graphene adsorption. The $[Li(DEE)_3(FSI)_1]$ complex is likely to be kinetically constrained at the interphase due to its ability to approach the interphase closer (Figure 4d), which implies the Li^+ enters the double layer at 213 K largely from $[Li(DEE)_2(FSI)_2]^-$ in the outer layer, similar to the $[Li(DME)_2(FSI)_1]$ complexes in the DOL/DME system at 298 K. It is also crucial to note that the change in total coordination number required for Li^+ to reach the inner layer is substantially different between electrolytes, where the 1 M LiFSI DEE electrolyte only requires a reduction of CN_{total} from 4 to 3. Conversely the DOL/DME system requires a CN_{total} from 6 to 3, thus placing a heightened "solution reorganization energy" on the system, indicative of highly thermal behavior (Figure S5). The illustrated desolvation processes for each system are shown in Figure 5, parts a and b, where the complexity of the DOL/DME system relative to the DEE electrolyte is clear.
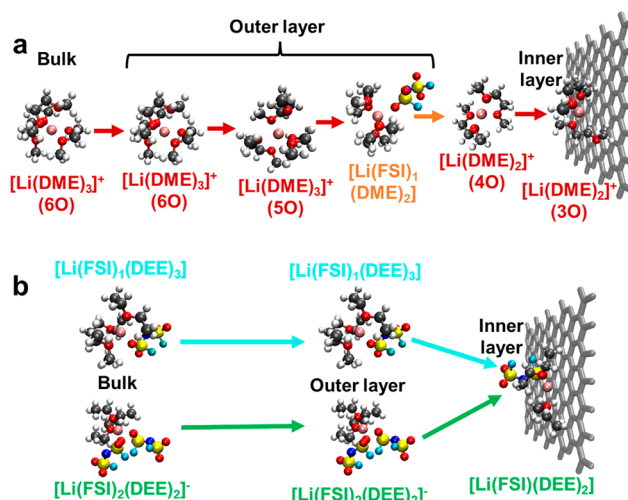
Figure 5. Visualized Li^+ desolvation process at 213 K in (a) 1 M LiFSI DOL/DME and (b) 1 M LiFSI DEE.

Though the desolvation processes investigated here are not specific to faradaic charge-transfer, the capacitive desolvation process shown here is analogous to previous charge-transfer models for metal plating.[32] Our previous work has shown that the consequence of the heightened temperature dependence of DME-based electrolytes leads to rapid cell failure at low temperatures,[14] which is problematic given that DME is a primary constituent of conventional electrolytes for Li metal and Li sulfur batteries.[12,20] Given the previously established conclusion that desolvation processes limit electrochemical

kinetics at low-temperatures, the differences in the predicted desolvation processes of the DOL/DME and DEE may be the mechanistic origin of their divergent behavior.[8,14,16,26] Moreover, this behavior is only understood through explicit free-energy sampling of the electrolyte/electrode phase space, which allows for the proposal of a charge-transfer route from the bulk-electrolyte to the inner Helmholtz layer. Though this work makes progress in doing so, a more sophisticated understanding of the interplay between solvation structure, interphase material, and corresponding ion-dynamics coupled with advanced experimental validation techniques at the interphase is necessary to fully understand the charge-transfer behavior in electrochemical systems.

■ ASSOCIATED CONTENT

ⓢ Supporting Information

The Supporting Information is available free of charge at https://pubs.acs.org/doi/10.1021/acs.jpclett.2c00770.

> Experimental methods, solvation analysis of bulk solvation from equilibrated MD simulations, deconvoluted density profiles of equilibrated MD simulations, 1D free energy profiles of total solvation number, 2D free energy profiles of neutral graphene at 213 K, 2D free energy profiles of charged graphene at 213 K as a function of total coordination number, and standard deviation of selected 2D free energy profiles (PDF)

■ AUTHOR INFORMATION

Corresponding Authors

Artem Baskin − *NASA Ames Research Center, Moffett Field, California 94035, United States;* ⓞ orcid.org/0000-0002-3156-6256; Email: abaskin@lbl.gov

Ping Liu − *Department of NanoEngineering, University of California, San Diego, La Jolla, California 92093, United States; Program of Chemical Engineering, Program of Materials Science and Engineering, and Sustainable Power and Energy Center, University of California, San Diego, La Jolla, California 92093, United States;* ⓞ orcid.org/0000-0002-1488-1668; Email: piliu@eng.ucsd.edu

Zheng Chen − *Department of NanoEngineering, University of California, San Diego, La Jolla, California 92093, United States; Program of Chemical Engineering, Program of Materials Science and Engineering, and Sustainable Power and Energy Center, University of California, San Diego, La Jolla, California 92093, United States;* ⓞ orcid.org/0000-0002-9186-4298; Email: zhengchen@eng.ucsd.edu

Authors

John Holoubek − *Department of NanoEngineering, University of California, San Diego, La Jolla, California 92093, United States;* ⓞ orcid.org/0000-0003-0015-4512

John W. Lawson − *NASA Ames Research Center, Moffett Field, California 94035, United States*

Hridayanand Khemchandani − *Department of NanoEngineering, University of California, San Diego, La Jolla, California 92093, United States;* ⓞ orcid.org/0000-0001-5722-0889

Tod A. Pascal − *Department of NanoEngineering, University of California, San Diego, La Jolla, California 92093, United States; Program of Chemical Engineering, Program of Materials Science and Engineering, and Sustainable Power and Energy Center, University of California, San Diego, La Jolla, California 92093, United States;* ⓞ orcid.org/0000-0003-2096-1143

Complete contact information is available at:
https://pubs.acs.org/10.1021/acs.jpclett.2c00770

Author Contributions

A.B. and J.H. conceived the idea and experimental plan. A.B., P.L., T.A.P., and Z.C. directed the project. J.H. and A.B. carried out the simulations. J.H., A.B., Z.C., P.L., and T.A.P wrote the paper. All authors discussed the results and commented on the manuscript.

Notes

The authors declare no competing financial interest.

■ ACKNOWLEDGMENTS

■ REFERENCES

(1) Liu, J.; Bao, Z.; Cui, Y.; Dufek, E. J.; Goodenough, J. B.; Khalifah, P.; Li, Q.; Liaw, B. Y.; Liu, P.; Manthiram, A.; Meng, Y. S.; Subramanian, V. R.; Toney, M. F.; Viswanathan, V. V.; Whittingham, M. S.; Xiao, J.; Xu, W.; Yang, J.; Yang, X.-Q.; Zhang, J.-G. Pathways for Practical High-Energy Long-Cycling Lithium Metal Batteries. *Nat. Energy* **2019**, *4* (3), 180−186.

(2) Weiss, M.; Ruess, R.; Kasnatscheew, J.; Levartovsky, Y.; Levy, N. R.; Minnmann, P.; Stolz, L.; Waldmann, T.; Wohlfahrt-Mehrens, M.; Aurbach, D.; Winter, M.; Ein-Eli, Y.; Janek, J. Fast Charging of Lithium-Ion Batteries: A Review of Materials Aspects. *Adv. Energy Mater.* **2021**, *11* (33), 2101126.

(3) Liu, Y.; Zhu, Y.; Cui, Y. Challenges and Opportunities towards Fast-Charging Battery Materials. *Nat. Energy* **2019**, *4* (7), 540−550.

(4) Gupta, A.; Manthiram, A. Designing Advanced Lithium-Based Batteries for Low-Temperature Conditions. *Adv. Energy Mater.* **2020**, *10* (38), 2001972.

(5) Logan, E. R.; Dahn, J. R. Electrolyte Design for Fast-Charging Li-Ion Batteries. *Trends in Chemistry* **2020**, *2* (4), 354−366.

(6) Logan, E. R.; Hall, D. S.; Cormier, M. M. E.; Taskovic, T.; Bauer, M.; Hamam, I.; Hebecker, H.; Molino, L.; Dahn, J. R. Ester-Based Electrolytes for Fast Charging of Energy Dense Lithium-Ion Batteries. *J. Phys. Chem. C* **2020**, *124* (23), 12269−12280.

(7) Chen, K.-H.; Namkoong, M. J.; Goel, V.; Yang, C.; Kazemiabnavi, S.; Mortuza, S. M.; Kazyak, E.; Mazumder, J.; Thornton, K.; Sakamoto, J.; Dasgupta, N. P. Efficient Fast-Charging of Lithium-Ion Batteries Enabled by Laser-Patterned Three-Dimensional Graphite Anode Architectures. *J. Power Sources* **2020**, *471*, 228475.

(8) Zhang, S. S.; Xu, K.; Jow, T. R. The Low Temperature Performance of Li-Ion Batteries. *J. Power Sources* **2003**, *115* (1), 137−140.

(9) Smart, M. C.; Ratnakumar, B. V.; Chin, K. B.; Whitcanack, L. D. Lithium-Ion Electrolytes Containing Ester Cosolvents for Improved Low Temperature Performance. *J. Electrochem. Soc.* **2010**, *157* (12), A1361−A1374.

(10) Li, Q.; Jiao, S.; Luo, L.; Ding, M. S.; Zheng, J.; Cartmell, S. S.; Wang, C.-M.; Xu, K.; Zhang, J.-G.; Xu, W. Wide-Temperature Electrolytes for Lithium-Ion Batteries. *ACS Appl. Mater. Interfaces* **2017**, *9* (22), 18826−18835.

(11) Dong, X.; Wang, Y.-G.; Xia, Y. Promoting Rechargeable Batteries Operated at Low Temperature. *Acc. Chem. Res.* **2021**, *54* (20), 3883−3894.

(12) Qian, J.; Henderson, W. A.; Xu, W.; Bhattacharya, P.; Engelhard, M.; Borodin, O.; Zhang, J.-G. High Rate and Stable Cycling of Lithium Metal Anode. *Nat. Commun.* **2015**, *6*, 6362.

(13) Liu, H.; Holoubek, J.; Zhou, H.; Chen, A.; Chang, N.; Wu, Z.; Yu, S.; Yan, Q.; Xing, X.; Li, Y.; Pascal, T. A.; Liu, P. Ultrahigh Coulombic Efficiency Electrolyte Enables Li‖SPAN Batteries with Superior Cycling Performance. *Mater. Today* **2021**, *42*, 17−28.

(14) Holoubek, J.; Liu, H.; Wu, Z.; Yin, Y.; Xing, X.; Cai, G.; Yu, S.; Zhou, H.; Pascal, T. A.; Chen, Z.; Liu, P. Tailoring Electrolyte Solvation for Li Metal Batteries Cycled at Ultra-Low Temperature. *Nature Energy* **2021**, *6* (3), 303−313.

(15) Xu, K. Charge-Transfer" Process at Graphite/Electrolyte Interface and the Solvation Sheath Structure of Li$^+$ in Nonaqueous Electrolytes. *J. Electrochem. Soc.* **2007**, *154* (3), A162.

(16) Xu, K.; von Cresce, A.; Lee, U. Differentiating Contributions to "Ion Transfer" Barrier from Interphasial Resistance and Li$^+$ Desolvation at Electrolyte/Graphite Interface. *Langmuir* **2010**, *26* (13), 11538−11543.

(17) Liao, B.; Li, H.; Xu, M.; Xing, L.; Liao, Y.; Ren, X.; Fan, W.; Yu, L.; Xu, K.; Li, W. Designing Low Impedance Interface Films Simultaneously on Anode and Cathode for High Energy Batteries. *Adv. Energy Mater.* **2018**, *8* (22), 1800802.

(18) Wen, B.; Deng, Z.; Tsai, P.-C.; Lebens-Higgins, Z. W.; Piper, L. F. J.; Ong, S. P.; Chiang, Y.-M. Ultrafast Ion Transport at a Cathode−Electrolyte Interface and Its Strong Dependence on Salt Solvation. *Nature Energy* **2020**, *5* (8), 578−586.

(19) Boyle, D. T.; Kong, X.; Pei, A.; Rudnicki, P. E.; Shi, F.; Huang, W.; Bao, Z.; Qin, J.; Cui, Y. Transient Voltammetry with Ultramicroelectrodes Reveals the Electron Transfer Kinetics of Lithium Metal Anodes. *ACS Energy Lett.* **2020**, *5* (3), 701−709.

(20) Cheng, H.; Sun, Q.; Li, L.; Zou, Y.; Wang, Y.; Cai, T.; Zhao, F.; Liu, G.; Ma, Z.; Wahyudi, W.; Li, Q.; Ming, J. Emerging Era of Electrolyte Solvation Structure and Interfacial Model in Batteries. *ACS Energy Lett.* **2022**, *7*, 490−513.

(21) Hou, S.; Ji, X.; Gaskell, K.; Wang, P.; Wang, L.; Xu, J.; Sun, R.; Borodin, O.; Wang, C. Solvation Sheath Reorganization Enables Divalent Metal Batteries with Fast Interfacial Charge Transfer Kinetics. *Science* **2021**, *374*, 172.

(22) Baskin, A.; Lawson, J. W.; Prendergast, D. Anion-Assisted Delivery of Multivalent Cations to Inert Electrodes. *J. Phys. Chem. Lett.* **2021**, *12* (18), 4347−4356.

(23) Aurbach, D.; Skaletsky, R.; Gofer, Y. The Electrochemical Behavior of Calcium Electrodes in a Few Organic Electrolytes. *J. Electrochem. Soc.* **1991**, *138* (12), 3536.

(24) Lu, Z.; Schechter, A.; Moshkovich, M.; Aurbach, D. On the Electrochemical Behavior of Magnesium Electrodes in Polar Aprotic Electrolyte Solutions. *J. Electroanal. Chem.* **1999**, *466* (2), 203−217.

(25) Lapidus, S. H.; Rajput, N. N.; Qu, X.; Chapman, K. W.; Persson, K. A.; Chupas, P. J. Solvation Structure and Energetics of Electrolytes for Multivalent Energy Storage. *Phys. Chem. Chem. Phys.* **2014**, *16* (40), 21941−21945.

(26) Li, Q.; Lu, D.; Zheng, J.; Jiao, S.; Luo, L.; Wang, C.-M.; Xu, K.; Zhang, J.-G.; Xu, W. Li+-Desolvation Dictating Lithium-Ion Battery's Low-Temperature Performances. *ACS Appl. Mater. Interfaces* **2017**, *9* (49), 42761−42768.

(27) Thenuwara, A. C.; Shetty, P. P.; McDowell, M. T. Distinct Nanoscale Interphases and Morphology of Lithium Metal Electrodes Operating at Low Temperatures. *Nano Lett.* **2019**, *19* (12), 8664−8672.

(28) Thenuwara, A. C.; Shetty, P. P.; Kondekar, N.; Sandoval, S. E.; Cavallaro, K.; May, R.; Yang, C.-T.; Marbella, L. E.; Qi, Y.; McDowell, M. T. Efficient Low-Temperature Cycling of Lithium Metal Anodes by Tailoring the Solid-Electrolyte Interphase. *ACS Energy Lett.* **2020**, *5* (7), 2411−2420.

(29) Derr, D. L.; Elliott, C. M. Temperature Dependence of the Outer-Sphere Reorganization Energy. *J. Phys. Chem. A* **1999**, *103* (39), 7888−7893.

(30) Marcus, R. A. On the Theory of Electron-Transfer Reactions. VI. Unified Treatment for Homogeneous and Electrode Reactions. *J. Chem. Phys.* **1965**, *43* (2), 679−701.

(31) Huang, B.; Myint, K. H.; Wang, Y.; Zhang, Y.; Rao, R. R.; Sun, J.; Muy, S.; Katayama, Y.; Corchado Garcia, J.; Fraggedakis, D.; Grossman, J. C.; Bazant, M. Z.; Xu, K.; Willard, A. P.; Shao-Horn, Y. Cation-Dependent Interfacial Structures and Kinetics for Outer-Sphere Electron-Transfer Reactions. *J. Phys. Chem. C* **2021**, *125* (8), 4397−4411.

(32) Wang, H.; Kim, S. C.; Rojas, T.; Zhu, Y.; Li, Y.; Ma, L.; Xu, K.; Ngo, A. T.; Cui, Y. Correlating Li-Ion Solvation Structures and Electrode Potential Temperature Coefficients. *J. Am. Chem. Soc.* **2021**, *143* (5), 2264−2271.

(33) Fan, X.; Ji, X.; Chen, L.; Chen, J.; Deng, T.; Han, F.; Yue, J.; Piao, N.; Wang, R.; Zhou, X.; Xiao, X.; Chen, L.; Wang, C. All-Temperature Batteries Enabled by Fluorinated Electrolytes with Non-Polar Solvents. *Nature Energy* **2019**, *4* (10), 882−890.

(34) Baskin, A.; Prendergast, D. Ion Solvation Spectra": Free Energy Analysis of Solvation Structures of Multivalent Cations in Aprotic Solvents. *J. Phys. Chem. Lett.* **2019**, *10* (17), 4920−4928.

(35) Baskin, A.; Prendergast, D. Ion Solvation Engineering: How to Manipulate the Multiplicity of the Coordination Environment of Multivalent Ions. *J. Phys. Chem. Lett.* **2020**, *11* (21), 9336−9343.

(36) Jorn, R.; Raguette, L.; Peart, S. Investigating the Mechanism of Lithium Transport at Solid Electrolyte Interphases. *J. Phys. Chem. C* **2020**, *124* (30), 16261−16270.

(37) Jorn, R.; Kumar, R.; Abraham, D. P.; Voth, G. A. Atomistic Modeling of the Electrode−Electrolyte Interface in Li-Ion Energy Storage Systems: Electrolyte Structuring. *J. Phys. Chem. C* **2013**, *117* (8), 3747−3761.

(38) Boyer, M. J.; Vilčiauskas, L.; Hwang, G. S. Structure and Li+ Ion Transport in a Mixed Carbonate/LiPF6 Electrolyte near Graphite Electrode Surfaces: A Molecular Dynamics Study. *Phys. Chem. Chem. Phys.* **2016**, *18* (40), 27868−27876.